phys. stat. sol. (b) **235**, No. 2, 354–359 (2003) / **DOI** 10.1002/pssb.200301621

Elastic properties and pressure-induced phase transitions of single-walled carbon nanotubes

S. Reich[*,1], **C. Thomsen**[1], and **P. Ordejón**[2]

[1] Institut für Festkörperphysik, Technische Universität Berlin, Hardenbergstr. 36, 10623 Berlin, Germany

[2] Institut de Ciència de Materials de Barcelona (CSIC), Campus de la U.A.B. 08193 Bellaterra, Barcelona, Spain

Received 5 August 2002, revised 2 December 2002, accepted 2 December 2002
Published online 4 February 2003

PACS 61.46.+w, 61.50.Ks

We studied the structure of single-walled carbon nanotubes under hydrostatic pressure by first-principles calculations. The circular tubes collapse at high pressure (7 GPa) to a phase with an elliptical cross-section. The elliptical structure leads to the formation of diamond-like bonds between the tubes at the point of strongest curvature. The bulk modulus of the circular, ambient-pressure phase that we found from our calculations is very similar to graphite (37 GPa). The interlinked phase also shows graphite-like behavior in the low- and high-pressure range: between 3.5 and 6.5 GPa its compressibility is very large. We compare our theoretical predicitions to X-ray scattering and piston–cylinder experiments.

1. Introduction The high-pressure behavior of carbon nanotubes has been studied with a variety of experimental techniques. Most of these studies seemed to indicate a phase transition of carbon under pressure, e.g., by X-ray [1, 2] a change in the bulk compressibility [3], the loss of the Raman [4–7] and absorption [8] intensity, or an increase in the resistivity [9, 10] under pressure. Although the experimental studies agree in some form of change of the ambient pressure phase, there is remarkable disagreement in the proposed transition pressures as well as the nature the new phase. For example, Tang et al. [1] reported the (10) X-ray diffraction peak to disappear around 1.5 GPa. Moreover, the change was irreversible if pressures above 5 GPa were applied to the sample. In contrast, Sharma et al. [2] observed a bundle X-ray peak up to 10 GPa. Similarly, the Raman spectrum of carbon nanotubes was found to remain unchanged after a pressure of 28 GPa was released [6].

To clarify the nature of the proposed phase transition the response of carbon nanotubes to hydrostatic external stress was simulated by total energy calculations ranging from empirical [7, 11] and semiempirical [4, 12] to first-principles methods [13–15]. The reported structures under high pressures were nanotubes with an elliptical or hexagonal cross-section. However, as mentioned for the experimental work, the results of the theoretical studies varied greatly with the specific nanotube under study and the applied method.

In this paper we report ab-initio calculations of carbon nanotubes under pressure. We calculate the elastic properties of the ambient pressure phase with an almost circular cross-section and compare them to experiment. We find that all studied nanotubes collapse under sufficiently high pressures and

[*] Corresponding author: e-mail: steffi@physik.tu-berlin.de

 0370-1972/03/23502-0354 $ 17.50+.50/0

form an oval shaped phase. This intermediate structure leads rapidly to an interlinking of the tubes at the points of strongest curvature. The transition pressure we observe depends on the chiralities of tubes, which in part explains the contradicting results.

2. Computational method The ambient pressure phase of carbon nanotubes consists of tubes with a circular or slightly hexagonally distorted cross-section arranged in hexagonally packed bundles. We simulated bundles of (6, 6), (10, 0), and (8, 4) nanotubes as infinite bulk crystals with a single tube in the unit cell. First-principles calculations were performed within the local density approximation [16] using the Siesta [17, 18] ab-initio package. Nonlocal, norm-conserving pseudopotentials [19] replaced the core electrons. The valence electrons were described by a double-ζ polarized basis set of localized orbitals with cutoff radii of 5.12 a.u. for the s and 6.25 a.u. for the p and d electrons obtained from an energy increase by 50 meV because of the localization [20, 21]. For real space integrations we used a regular grid corresponding to a plane-wave cutoff of $\approx$240 Ry. The metallic bundles of (6, 6) and (10, 0) nanotubes were calculated on a $2 \times 2 \times 30$ and $2 \times 2 \times 10$ Monkhorst-Pack grid in reciprocal space. Only the Γ point was used for the bundle of chiral (8, 4) nanotubes [22].

To find the lattice parameters and the atomic positions at a given pressure point we performed a conjugate gradient minimization under the constrained of a hydrostatic stress tensor. In contrast to previous studies where only the bundle lattice constants perpendicular to the axis were modified to mimic the hydrostatic pressure situation [12, 13], we are thus able to study the changes along the nanotube z-axis as well. The conjugate gradient relaxation was considered converged if the forces on the atoms were below 5 meV/Å and every stress tensor component within 5–10% of the imposed value, i.e., tolerating differences between 0.02 GPa at zero pressure and 1 GPa at 25 GPa, the highest pressure point.

3. Results and discussion In this section, we first present the elastic properties of the ambient pressure phase before turning to phase transitions in carbon nanotubes under high pressure.

3.1 Ambient pressure phase The elastic properties of the ambient pressure phase are summarized in Fig. 1. The volume of the unit cell (labeled bundle unit cell in Fig. 1) shows a sublinear pressure dependence with a bulk modulus of $B_0^{\mathrm{b}} = 37$ GPa at zero pressure and its first derivative $B' = 11$. These values are practically the same as those for graphite (39 GPa and 10 with the same basis set) and are also in agreement with published empirical calculations [11, 25]. Included in Fig. 1 are also the experimental data points obtained by Tang et al. [1] and Sharma et al. [2] which agree excellently with the ab-initio results [24]. The volume change for the individual tubes within the bundles is shown in the lower trace of Fig. 1 (individual tubes). Every single tube has a linear pressure dependence with a bulk modulus of 230 GPa. Since the deformation of the individual tubes reflects the changes in lengths and angles of the carbon bonds forming the nanotube wall, Raman scattering probes mostly

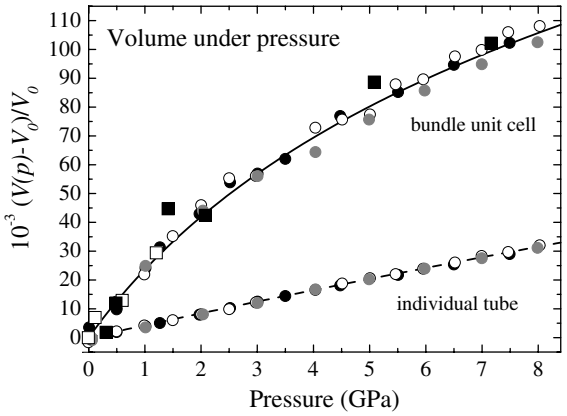

Fig. 1 Volume dependence of the bundle unit cell and the individual tubes within the bundle as a function of applied pressure. The dots were obtained from our ab-initio calculations: open dots are for the (10, 0), closed black dots for the (6, 6), and gray dots for the (8, 4) nanotube bundle. The lines represent fits using the equation of state by Vinet et al. [23]. Open squares are the experimental results by Tang et al. [1] and closed squares the ones by Sharma et al. [2] (from Ref. [24]).

the intratube contributions of the pressure dependence [4, 6, 26]. This holds in particular for the high-energy modes around 1600 cm^{-1}, whereas the pressure slope of the radial breathing mode is determined by the intertube as well as the intratube contributions [4, 5]. In Ref. [24] we analyzed the linear compressibilities along the nanotube axis and in the radial direction in more detail. We showed that the behavior of the individual tubes in the ambient pressure phase is very well described by macroscopic continuum mechanics [27].

3.2 Phase transitions under pressure The volume compressibility at zero pressure is much larger for the bundle (27 TPa^{-1}) than for the individual tubes (4.4 TPa^{-1}). Therefore, at low pressure mostly the distance between the tube is reduced by the external forces. The compressibility of the bundle decreases rapidly with increasing pressure: at 10 GPa it is reduced to 5.0 TPa^{-1} in our calculation. This decrease is the driving force for the structural changes, which reduce the empty volume inside the tube.

Up to 8 GPa the circular phase of all three nanotube bundles was stable. The cross-section of the tubes was slightly hexagonally distorted (between $< 1\%$ radius deviations at ambient pressure and 5% at 8 GPa). The distortion had, however, no significant effect on the calculated phonon spectrum or the electronic band structure along the reciprocal z-axis. At 9 GPa applied external pressure, the armchair tubes collapsed to an elliptical phase [3, 7, 15]. This intermediate phase was unstable when the pressure was further increased to 10.5 GPa and replaced by a phase where the flattened tubes were connected by carbon–carbon bonds. In Fig. 2a we show the structures of the ambient pressure phase, the elliptical phase in Fig. 2b, and the interlinked phase in Fig. 2c at a pressure of 6.5 GPa. The elliptical cross-section is favored at high pressure because the unit cell volume is reduced by $\approx 5\%$. On the other hand, it requires a strong bending of the graphene sheet and thus a large strain energy. In the interlinked phase in Fig. 2c the strain is almost released from the individual tubes. The sidewalls are straight, resembling graphite, whereas the contact points are formed by sp^3 diamond-like bonds. The angles of interlinking bonds are 112.9°, 101.6°, and 114.7°. The elliptical phase is unstable to a circular distortion at low pressure, while at high pressures tube–tube bonds are formed releasing the large bending strains.

In Fig. 3 we show the total energy of the three phases versus the unit cell volume. The elliptical tubes have higher total energies than either the circular or the interlinked phase. The barrier between the elliptical and the interlinked tube phase seems to be very small, since we rapidly (1.5 GPa further pressure increase) obtained the interlinked structure once the tubes collapsed. For the (6, 6) nanotubes the interlinked structure was metastable under the release of the pressure down to zero pressure. We could only follow the elliptical phase between 5 and 10.5 GPa. From the total energy curves in Fig. 3 we calculated the enthalpies as a function of pressure and found an expected transition pressure (equilibrium of the enthalpies) between the circular and the elliptical tubes of 7 GPa. However, for

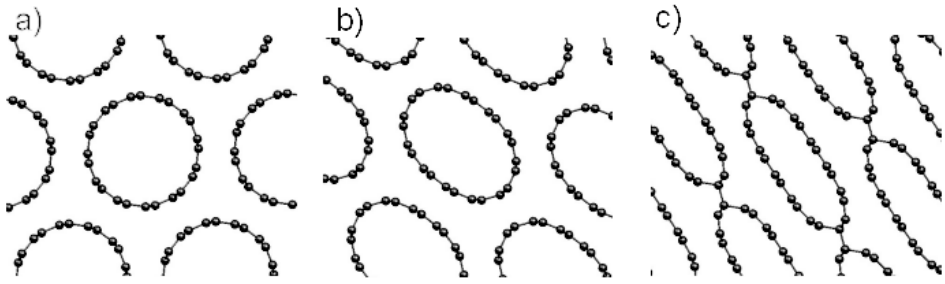

Fig. 2 Ambient and high-pressure phases of a (6, 6) nanotube bundle at 6.5 GPa. a) Ambient-pressure phase with a slightly hexagonally distorted circular cross-section of the nanotubes. b) High-pressure phase with an elliptical cross-section. From the enthalpy the transition pressure between the ambient and this collapsed phase is estimated as 7 GPa. c) Interlinked phase, which has the lowest enthalpy above 3.5 GPa. While the tube wall is composed of graphene-like sp^2 bonds, the bond connecting to two tubes has mostly sp^3 diamond-like character.

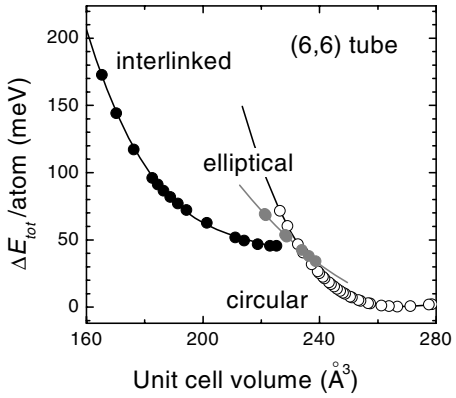

Fig. 3 Total energy of the (6, 6) nanotubes as a function of unit cell volume. Open dots are the energies of the circular phase in Fig. 2a, gray dots of the elliptical tubes in Fig. 2b, and closed black dots for the interlinked structure in Fig. 2c. The lines are cubic fits to the total energy curves.

pressures above 3.5 GPa the interlinked phase is lower in enthalpy than the two other phases. The collapse of the tubes is a necessary intermediate step for the formation of the carbon–carbon bonds between two tubes in close contact. The higher transition pressure for the flattening of the tubes postpones the transition to the interlinked phase. The transitions pressures we obtained from the first-principles calculation are in reasonable agreement with the experimentally observed decrease in the radial breathing mode intensity between 2 and 4 GPa in Raman scattering [4–7] and the increase in resistivity at 2 GPa [10]. In particular, when taking into account that the experiments were performed on larger diameter tubes, $d \approx 1.5$ nm in contrast to the $d = 0.8$ nm tubes in our calculations.

In the (8, 4) and the (10, 0) bundle the ambient pressure phase was stable up to 12 GPa. For 15 GPa applied pressure the tubes collapsed to the elliptical cross-section and immediately started to form bonds between the tubes. A flattening of the tubes occurs regardless of their chirality under pressure in contrast to the symmetry driven phase transformation proposed by Sluiter et al. [15]. Also, the tube–tube interlinking is not restricted to the high-symmetry achiral tubes. Further calculations for the chiral and zig-zag tubes are needed to clarify the transition path.

3.3 Elastic properties of the high-pressure phase The volume dependence of the interlinked phase on pressure is shown in Fig. 4. The inset depicts the interlinked tubes at zero external pressure. The dots are the calculated volumes normalized to the zero pressure value (225 Å^3). The dashed line was obtained from the pressure dependence of the circular tubes. The interlinked phase has the same bulk modulus as the circular tubes below 3.5 GPa. Between 3.5 and 6.5 GPa the volume decreases rapidly.

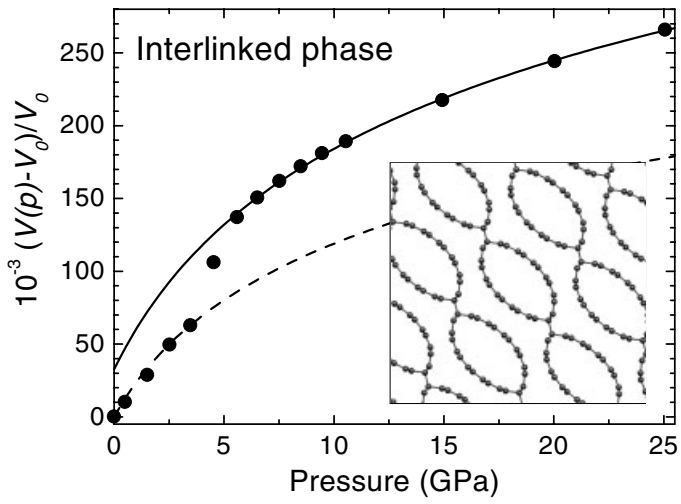

Fig. 4 Normalized volume of the interlinked tubes as a function of pressure. The dashed line corresponds to the volume pressure dependence of the ambient pressure phase with a circular cross-section. It was obtained from Fig. 1. The solid line is a fit with the Vinet equation to the calculated volumes between 6.5 and 25 GPa. The inset shows the zero-pressure structure of the interlinked phase, which we found to be metastable upon release of the pressure.

Above 6.5 GPa the elastic properties of the interlinked phase are again very similar to the circular phase and graphite with a bulk modulus $B_0 = 31$ GPa and its first derivative $B' = 6.7$. The reason for these three different regimes becomes apparent when looking at the relaxed structures. Between 0 and 3.5 GPa the elastic properties of the interlinked phase are as for the circular phase determined by the weak van-der-Waals interaction between the tubes. The tubes get closer together without observable changes in their shape. Around 4 GPa it becomes favorable to deform the tubes until they are completely flat at 6.5 GPa as can be seen in Fig. 2c. A further increase in pressure leads again to a graphitic behavior. The abrupt change in the elastic response of the interlinked tubes confirms the transition pressure from the enthalpy differences of the three phases.

A strongly elliptical cross-section of carbon nanotubes under pressure was first proposed by Chesnokov et al. [3]. They proposed this structure because of the very low bulk modulus ($B_0 = 3$ GPa and $B' = 5.5$) they obtained in a piston-cylinder experiment. The volume reduction in Fig. 2 of Ref. [3], however, shows neither the low- nor the high-pressure van-der-Waals dominated regime. For the higher-pressure regime, i.e., totally flattened tubes, this is understandable, since the pressures realized by Chesnokov et al. [3] were below 3 GPa. For small pressures a possible explanation is a flattening of their tubes at much lower pressure because of the larger diameters of the experimentally studied tubes. On the other hand, an immediate flattening of all tubes below 2 GPa contradicts the diamond-anvil measurements. Since the transition pressure depends on the diameters and the chiralities of the tubes, the different phases might coexist over a wide pressure range. Raman and X-ray scattering probe mostly the ambient pressure phases, which is in agreement with the intensity loss observed in scattering experiments.

4. Conclusion In conclusion, we studied the structure of single-walled nanotubes under pressures up to 20 GPa by ab-initio calculations. The circular cross-section of the 8 Å diameter tubes collapses between 9 and 15 GPa to an oval shape. A further increase of the applied pressure yielded an interlinked phase where diamond-like bonds are formed between the tubes. The critical pressure for the phase transition depends on the chirality of the tube. For a bundle of (6, 6) tubes the transition occurs at 7 GPa. We calculated the elastic properties of the circular and the interlinked phase and found them to be similar to graphite for most of the pressures. Finally, we discussed the experimental evidence for phase transitions in carbon nanotubes. Despite the wealth of experimental and theoretical studies on the subject, further work is needed to clarify the high-pressure behavior of single-walled carbon nanotubes.

References

[1] J. Tang, L.-C. Qin, T. Sasaki, M. Yudasaka, A. Matsushita, and S. Iijima, Phys. Rev. Lett. **85**, 1887 (2000).
[2] S. M. Sharma, S. Karmakar, S. K. Sikka, P. V. Teredesai, A. K. Sood, A. Govindaraj, and C. N. R. Rao, Phys. Rev. B **63**, 205417 (2001).
[3] S. A. Chesnokov, V. A. Nalimova, A. G. Rinzler, R. E. Smalley, and J. E. Fischer, Phys. Rev. Lett. **82**, 343 (1999).
[4] U. D. Venkateswaran, A. M. Rao, E. Richter, M. Menon, A. Rinzler, R. E. Smalley, and P. C. Eklund, Phys. Rev. B **59**, 10 928 (1999).
[5] C. Thomsen, S. Reich, A. R. Goñi, H. Jantoljak, P. Rafailov, I. Loa, K. Syassen, C. Journet, and P. Bernier, phys. stat. sol. (b) **215**, 435 (1999).
[6] A. K. Sood, P. V. Teresdesai, D. V. S. Muthu, R. Sen, A. Govindaraj, and C. N. R. Rao, phys. stat. sol. (b) **215**, 393 (1999).
[7] M. J. Peters, L. E. McNeila, J. P. Lu, and D. Kahn, Phys. Rev. B **61**, 5939 (2000).
[8] S. Kazaoui, N. Minami, H. Yamawaki, K. Aoki, H. Kataura, and Y. Achiba, Phys. Rev. B **62**, 1643 (2000).
[9] A. D. Bozhko, D. E. Slovsky, V. A. Nalimova, A. G. Rinzler, R. E. Smalley, and J. E. Fischer, Appl. Phys. A: Mater. Sci. Process. **67**, 75 (1998).
[10] R. Gaál, J.-P. Salvetat, and L. Forró, Phys. Rev. B **61**, 7320 (2000).
[11] L. A. Girifalco, M. Hodak, and R. S. Lee, Phys. Rev. B **62**, 13104 (2000).
[12] D. Kahn and J. P. Lu, Phys. Rev. B **60**, 6535 (1999).

[13] T. Yildirim, O. Gülseren, Ç. Kılıç, and S. Ciraci, Phys. Rev. B **62**, 12648 (2000).
[14] S. Okada, A. Oshiyama, and S. Saito, J. Phys. Soc. Jpn. **70**, 2345 (2001).
[15] M. H. F. Sluiter, V. Kumar, and Y. Kawazoe, Phys. Rev. B **65**, 161402 (2002).
[16] J. P. Perdew and A. Zunger, Phys. Rev. B **23**, 5048 (1981).
[17] D. Sánchez-Portal, P. Ordejón, E. Artacho, and J. M. Soler, Int. J. Quantum Chem. **65**, 453 (1997).
[18] J. M. Soler, E. Artacho, J. D. Gale, A. García, J. Junquera, P. Ordejón, and D. Sánchez-Portal, J. Phys.: Condens. Matter **14**, 2745 (2002). Cond-mat/0111138.
[19] N. Troullier and J. L. Martins, Phys. Rev. B **43**, 1993 (1991).
[20] E. Artacho, D. Sánchez-Portal, P. Ordejón, A. García, and J. Soler, phys. stat. sol. (b) **215**, 809 (1999).
[21] J. Junquera, O. Paz, D. Sánchez-Portal, and E. Artacho, Phys. Rev. B **64**, 235111 (2001).
[22] S. Reich, C. Thomsen, and P. Ordejón, Phys. Rev. B **65**, 155411 (2002).
[23] P. Vinet, J. H. Rose, J. Ferrantes, and J. R. Smith, J. Phys.: Condens. Matter **1**, 1941 (1989).
[24] S. Reich, C. Thomsen, and P. Ordejón, Phys. Rev. B **65**, 153407 (2002).
[25] M. Popov, M. Kyotani, R. J. Nemanich, and Y. Koga, Phys. Rev. B **65**, 033408 (2002).
[26] S. Reich, C. Thomsen, G. S. Duesberg, and S. Roth, Phys. Rev. B **63**, R041401 (2001).
[27] C. Thomsen, S. Reich, H. Jantoljak, I. Loa, K. Syassen, M. Burghard, G. S. Duesberg, and S. Roth, Appl. Phys. A **69**, 309 (1999).